J Solid State Electrochem (2012) 16:1447–1452
DOI 10.1007/s10008-011-1467-8

ORIGINAL PAPER

Nano-sized $La_{0.8}Sr_{0.2}MnO_3$ as oxygen reduction catalyst in nonaqueous Li/O_2 batteries

Zhenghao Fu · Xiujing Lin · Tao Huang · Aishui Yu

Received: 15 April 2011 / Revised: 4 June 2011 / Accepted: 7 June 2011 / Published online: 27 September 2011

Abstract Nano-sized $La_{0.8}Sr_{0.2}MnO_3$ prepared by the polyethylene glycol assisting sol–gel method was applied as oxygen reduction catalyst in nonaqueous Li/O_2 batteries. The as-synthesized $La_{0.8}Sr_{0.2}MnO_3$ was characterized by X-ray diffraction (XRD), scanning electron microscopy, and Brunauer–Emmet–Teller measurements. The XRD results indicate that the sample possesses a pure perovskite-type crystal structure, even sintered at a temperature as low as 600 °C, whereas for solid-state reaction method it can only be synthesized above 1,200 °C. The as-prepared nano-sized $La_{0.8}Sr_{0.2}MnO_3$ has a specific surface area of 32 $m^2\ g^{-1}$, which is much larger than the solid-state one (1 $m^2\ g^{-1}$), and smaller particle size of about 100 nm. Electrochemical results show that the nano-sized $La_{0.8}Sr_{0.2}MnO_3$ has better catalytic activity for oxygen reduction, higher discharge plateau and specific capacity.

Keywords Sol–gel · Solid-state reaction · Li/O_2 · Catalytic activity

Introduction

Lithium/air batteries can achieve a much higher energy density and are safer than most commercial lithium batteries, concluding rechargeable lithium ion battery. By using ambient air as the oxidant, if the air is excluded, a Li/air battery can deliver rather high energy density, which is five to ten times higher than that of a lithium ion battery [1–4]. Lithium–air batteries base on the two reactions: $2Li+O_2 \rightarrow 2Li_2O_2$, $E=3.10$ V or $4Li+O_2 \rightarrow 2Li_2O$, $E=2.91$ V [5], which has an open circuit voltage of about 3 V, and high theoretical capacity is of 5,200 Wh kg^{-1} (first reported by Abraham and Jiang in 1996 [6]). However, there are still some drawbacks limiting its application, including the polarization of oxygen reduction reaction, the volatile and decomposition of organic electrolyte, lithium oxides insoluble in the organic electrolyte, etc. [7, 8]. Up to now, many works have been made to solve these problems. Presently, most studies are focused on these three aspects: (1) Li–air cells with liquid and solid electrolytes, (2) porous electrode materials and structures and cell performance evaluation, and (3) catalysis of cell reactions [9]. Lots of works proved that the performance of Li–air batteries can be drastically improved by incorporating an effective catalyst, achieving higher discharge voltage and rate [10–13]. Therefore, developing novel catalysts with high catalytic activities for oxygen reduction reaction (ORR) is significant.

The mix metal perovskite $La_{0.8}Sr_{0.2}MnO_3$ is a classical catalytic material used as a catalyst for oxygen reduction in fuel cell due to its high catalytic activity and stability [14–16]. It shows better performance among other perovskite oxides through intensive studying on rare earth and 3D transition element [17] plus it is cheaper than noble metal catalyst such as Au and Pt. More recently, it has been incorporated in Li/O_2 batteries as an ORR catalyst [10] but no supporting information about synthesis was provided by Debart et al. However, this material is very hard to synthesize. Its high temperature demand and ability to generate impurities easily, which leads to low specific surface area (generally less than 10 $m^2\ g^{-1}$) and low catalytic activity, thus limited its usage. Since the morphologies (particle size and particle shape-specific surface area) are

Z. Fu · X. Lin · T. Huang · A. Yu (✉)
Department of Chemistry, Shanghai Key Laboratory of Molecular Catalysis and Innovative Materials, Institute of New Energy, Fudan University,
Shanghai 200438, China
e-mail: asyu@fudan.edu.cn

important factors for its catalytic activity [18], it is significant to synthesize perovskite $La_{0.8}Sr_{0.2}MnO_3$ with high purity and nano-sized particles [19–23].

Herein, we systematically describe a soft chemistry method for a successful synthesis of nano-sized $La_{0.8}Sr_{0.2}MnO_3$ and make a scrutiny into the catalysis effect of $La_{0.8}Sr_{0.2}MnO_3$; in this method, only two steps are applied to synthesized this nano-sized $La_{0.8}Sr_{0.2}MnO_3$ (LSMO): first, sol–gel assisted with polyethylene glycol (PEG) and second, the sinter temperature is only 600 °C (which is much lower than a solid-state one). As a heterogeneous phase catalyst, the electrocatalytic activities of the as-prepared $La_{0.8}Sr_{0.2}MnO_3$ materials for oxygen reduction reaction and their electrochemical performance in using lithium–air batteries were investigated. At the same time, the high temperature solid-state reaction method synthesized $La_{0.8}Sr_{0.2}MnO_3$ is also studied as a comparison.

Experimental section

Synthesis of $La_{0.8}Sr_{0.2}MnO_3$

The synthesis of g-$La_{0.8}Sr_{0.2}MnO_3$ nano-particles was carried out by a sol–gel method associated with the PEG. Sol–gel materials were prepared from metal nitrate solution by the PEG assisting method. Gels are obtained by dissolving the appropriate amounts of metal nitrate and citric acid in de-ionized water at room temperature followed by stirring for 10 min. $NH_3{\cdot}H_2O$ was added slowly to adjust the pH to 8 and then stirred for 30 min to chelate completely. At last PEG-2000 was added and the solutions were stirred vigorously until gel occurred. A typical $La_{0.8}Sr_{0.2}MnO_3$ gel was obtained by mixing La $(NO_3)_2{\cdot}6H_2O$ (1.333 g), $Sr(NO_3)_3$ (0.164 g), $Mn(NO_3)_2$ (1.378 g), $C_6H_6O_7{\cdot}2H_2O$ (3.514 g), and PEG-2000 (0.574 g), and the mol ratio of metallic ions ($La^{3+}/Sr^{2+}/Mn^{2+}$) was 0.8/0.2/1.

The precursor was dried under vacuum at 80 °C for 12 h. After being milled, the sample was transferred into a muffle stove with a temperature of 220 °C for 1 h (a heating rate of 10 °C min^{-1}) then increased to 600 °C (heating rate, 5 °C min^{-1}) and sintered for 2 h.

For comparison, s-$La_{0.8}Sr_{0.2}MnO_3$ was prepared with solid-state reaction method based on the previous study of D. Grossin's group [23]. The starting chemical pure lanthanum oxide (La_2O_3 (AR grade)), strontium carbonate ($SrCO_3$ (AR grade)), and manganese oxide (MnO_2 (AR grade)) reagents have been mixed according to the stoichiometric ratios using agate container and semi-planetary grinder (Fritsch) set-up for 45 min; the resulting mixture was heated (1,200 °C, 12 h in air) to form LSMO powder with a nominal composition of $La_{0.8}Sr_{0.2}MnO_3$; 1.3032 g of La_2O_3, 0.8690 g of MnO_2, and 0.2953 g of $SrCO_3$ were transferred into an agate container and were milled at a grinding speed of 250 $rmin^{-1}$ for 45 min. Finally, the mixture was sintered at 1,200 °C in air for 12 h.

PEG-2000 (CP grade), $La(NO_3)_2{\cdot}6H_2O$, $Sr(NO_3)_3$, Mn $(NO_3)_2$ (50 wt.% solution), $C_6H_6O_7{\cdot}2H_2O$, $NH_3{\cdot}H_2O$ (25%), La_2O_3, and $SrCO_3$ were purchased from Sinopharm Chemical reagent Co., MnO_2 (from TOSOH, Japan), and all of them were of AR grade.

Material characterization and electrochemical measurement

Powder XRD measurement was performed on a Bruker D8 Advance with Cu Kα radiation at a rate of 4°min^{-1}. scanning electron microscopy (SEM) image were obtained on JEOL JSM-6390 operated at 20 kV. Brunauer–Emmet–Teller (BET) surface areas using nitrogen adsorption–desorption measurements were performed on a Quantachrome Instruments at 77 K.

Electrocatalytic activity was investigated by cyclic voltammetry performed in a three-electrode system. Sample was prepared by mixing catalyst and Super P in a 1:1 ratio, and 10 mg mixture was dispersed in 2 mL isopropanol under ultrasonic action; after 10 min, take 5 μL mixture using Nafion coated on a diameter of 5 mm GC electrodes as the working electrode, SCE as the reference electrode, and a Pt foil as the auxiliary electrode. Cycling voltammetry was conducted on an electrochemical workstation (CHI 660C, CH Instrument company). The electrolyte, 1 mol/L KOH solution, was first bubbled with N_2 for at least 30 min to

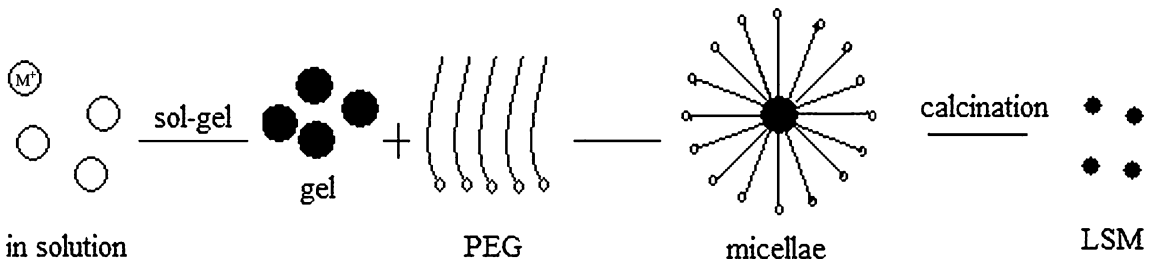

Scheme 1 The formation process of g-$La_{0.8}Sr_{0.2}MnO_3$ particles

make the solution saturated with N_2, tested from 0.2 to −0.8 V versus SCE at a scan rate of 50 mV s^{-1}, and then purged with O_2 for 30 min; the experiment was repeated.

Air cathode was prepared and Li–air battery was measured following the methods. The catalyst mixed with Super P was used as the cathode materials to catalyze O_2 reduction. For this study, Swagelok cell was incorporated. Lithium metal foil with a thickness of 0.60 mm was used as the anode; the foil was pressed on the stainless steel current collector. Air cathode was made by depositing the slurry on a carbon paper. It is a multilayer structure with the first layer (powdered carbon layer) made by combing super P, PTFE with a weight ratio of 1:1. The second layer (catalyst layer) was mix with super P, PTFE, catalyst at a ratio of 5:4:1. This structure was then wrapped around a steel current collector. The air hole is 0.785 cm^2 to let the oxygen flow in. The nonaqueous electrolyte consisted of a solution of 1 M $LiPF_6$ in 1:1 volume EC/DMC (Jiangsu Guotai Huarong Chemical Corp). The cell was assembled in the glove box filled with argon. And then the cell was cycled on a LAND cycler (Wuhan Jinnuo Electronic Co. Ltd.) in a container keeping oxygen flow at room temperature.

Results and discussion

Scheme 1 illustrated the route for the g-$La_{0.8}Sr_{0.2}MnO_3$ formation. The surfactant PEG-2000 was adsorbed on the gel surface and then forms micelle preventing the particles conglobation from growing up. It keeps uniform size and results in small particle size and large specific surface area, which will be proved by the SEM image and BET data. As

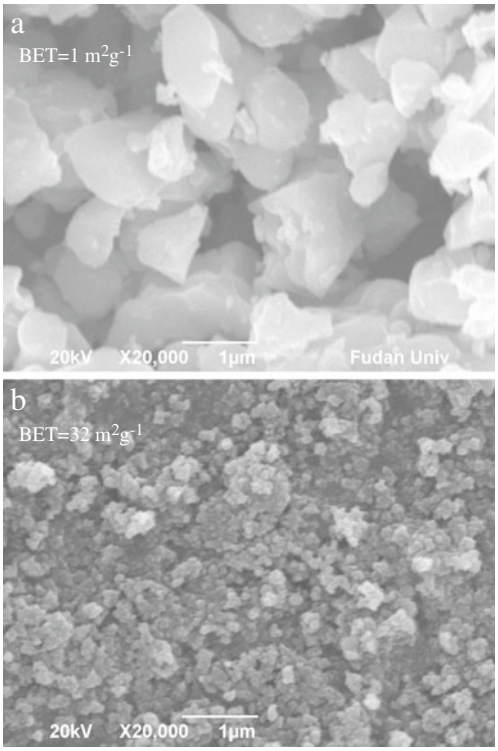

Fig. 2 The specific BET surface areas and particle sizes of the two as-synthesis $La_{0.8}Sr_{0.2}MnO_3$: **a** s-$La_{0.8}Sr_{0.2}MnO_3$ and **b** g-$La_{0.8}Sr_{0.2}MnO_3$

to the s-$La_{0.8}Sr_{0.2}MnO_3$, the particles agglomerated at high temperature, and made the particle size get bigger leading to small specific surface area.

Figure 1 presents the XRD patterns of (a) s-$La_{0.8}Sr_{0.2}MnO_3$, (b) g-$La_{0.8}Sr_{0.2}MnO_3$ and (c) standard XRD pattern of

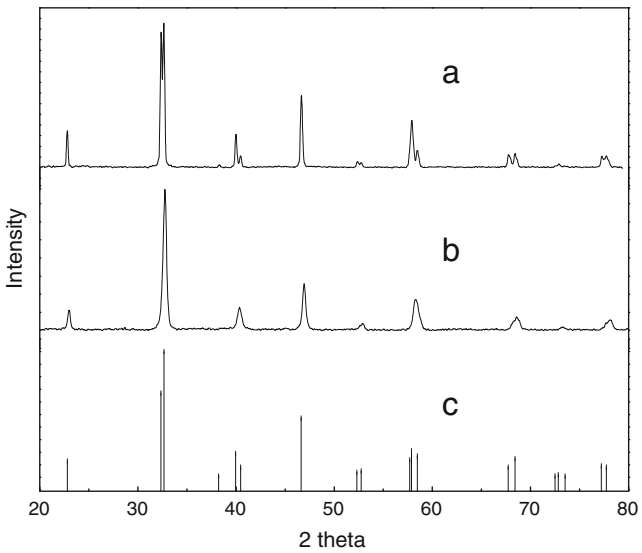

Fig. 1 The XRD patterns of $La_{0.8}Sr_{0.2}MnO_3$: *a* s-$La_{0.8}Sr_{0.2}MnO_3$, *b* g-$La_{0.8}Sr_{0.2}MnO_3$, and *c* the standard XRD pattern of $La_{0.8}Sr_{0.2}MnO_3$

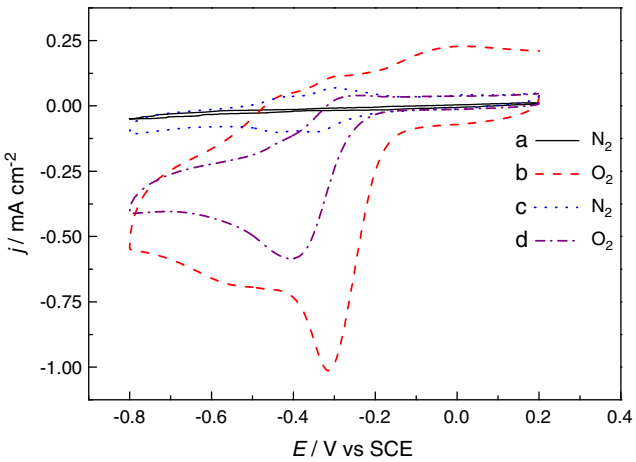

Fig. 3 The cycling voltammogram curve of two kinds of $La_{0.8}Sr_{0.2}MnO_3$-catalyzed glass carbon electrode between voltage limits 0.2 to −0.8 V at a scanning rate of 50 mV s^{-1}: *a* g-$La_{0.8}Sr_{0.2}MnO_3$ in N_2-saturated solution, *b* g-$La_{0.8}Sr_{0.2}MnO_3$ in O_2-saturated solution, *c* s-$La_{0.8}Sr_{0.2}MnO_3$ in N_2-saturated solution, and *d* s-$La_{0.8}Sr_{0.2}MnO_3$ in O_2-saturated solution

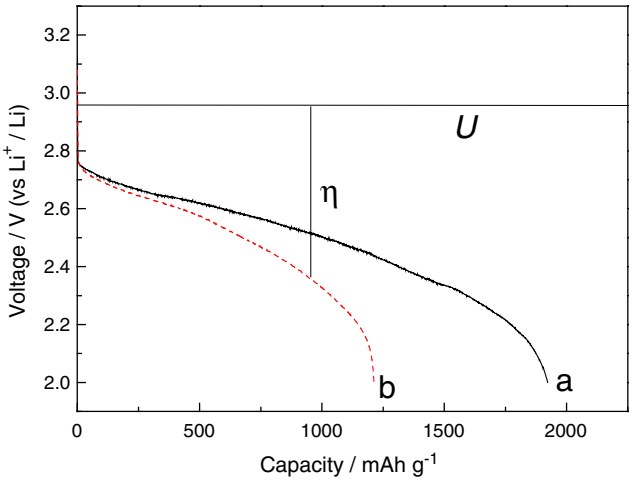

Fig. 4 The discharge curve of non-catalyst and g-$La_{0.8}Sr_{0.2}MnO_3$-catalyzed Li–air battery: *a* g-$La_{0.8}Sr_{0.2}MnO_3$-catalyzed air cathode and *b* is the s-$La_{0.8}Sr_{0.2}MnO_3$ catalysis cathode

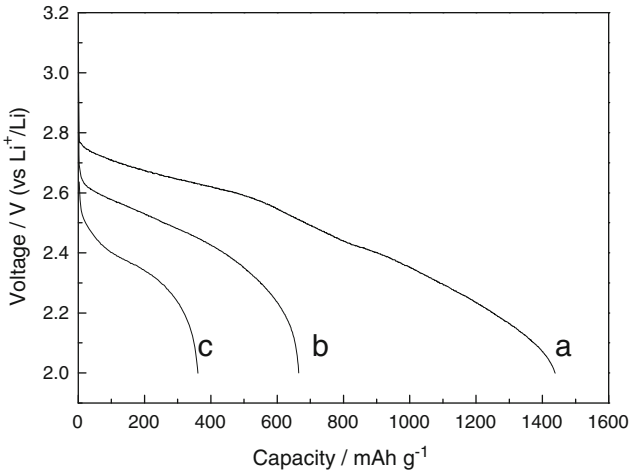

Fig. 6 Discharge curve of the Li/air battery incorporated s-$La_{0.8}Sr_{0.2}MnO_3$: *a* 0.1, *b* 0.2, and *c* 0.5 mA cm^{-2}

$La_{0.8}Sr_{0.2}MnO_3$ (JCPDS 40–1100). It can be seen that all the diffraction peaks in Fig. 1a, b can be attributed to $La_{0.8}Sr_{0.2}MnO_3$, which agrees well with that previously reported in Ref. [24]. All the samples are perovskites phase and with a rhombohedral structure. No any other peaks can be observed, illustrating that the samples were comparatively pure with less impurities. What's more, the diffraction peaks in curve (a) are sharper and more stronger than those in curve (b). The possible reason is that the s-$La_{0.8}Sr_{0.2}MnO_3$ annealed at 1,200 °C which leads to higher crystallinity and bigger particle size than that prepared by the sol–gel method.

The morphology is characterized by SEM. Figure 2 shows the SEM images of (a) s-$La_{0.8}Sr_{0.2}MnO_3$ and (b) g-$La_{0.8}Sr_{0.2}MnO_3$. It can be seen that the particle size of s-$La_{0.8}Sr_{0.2}MnO_3$ is about 1–3 μm. However, g-$La_{0.8}Sr_{0.2}MnO_3$ has a uniform size of about 100 nm, which is much smaller than that of the s-$La_{0.8}Sr_{0.2}MnO_3$. Furthermore, severe agglomeration can be seen in s-$La_{0.8}Sr_{0.2}MnO_3$. However, for g-$La_{0.8}Sr_{0.2}MnO_3$, it has good dispersion. The smaller particle size and good dispersion might lead to higher specific surface area, which is very important for its electrocatalytic activity for oxygen reduction reaction.

The BET specific surface areas detected by nitrogen adsorption–desorption measurements of g-$La_{0.8}Sr_{0.2}MnO_3$ and s-$La_{0.8}Sr_{0.2}MnO_3$ are 32 and 1 $m^2\ g^{-1}$, respectively. It demonstrates that sol–gel method assisted by PEG is a better route to synthesize nano-sized $La_{0.8}Sr_{0.2}MnO_3$ with higher specific surface area than the solid-state method.

Figure 3 shows the CV curves of the as-prepared $La_{0.8}Sr_{0.2}MnO_3$ materials in N_2-saturated or O_2-saturated 1 mol L^{-1} KOH solution at a sweep rate of 50 mV s^{-1}. From curve a, it can be seen that there is no peak between 0.20 and −0.80 V, further indicating that the $La_{0.8}Sr_{0.2}MnO_3$ material prepared by sol–gel method is pure without any other impurities. However, for $La_{0.8}Sr_{0.2}MnO_3$ material prepared by solid-state method, one pair peaks in curve c can be observed, demonstrating that there are some

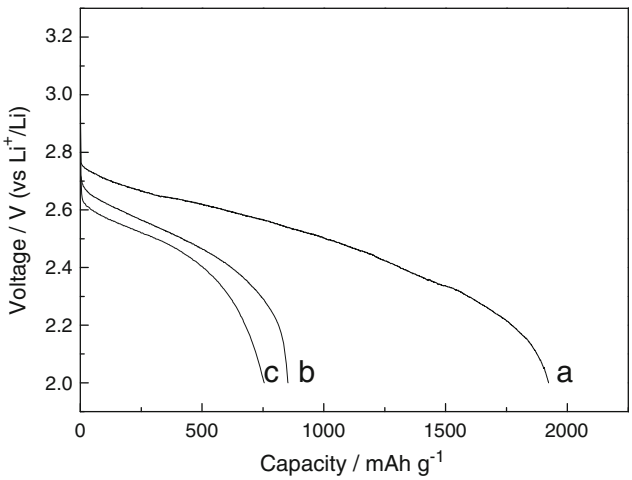

Fig. 5 Discharge curve of the Li/air battery incorporated g-$La_{0.8}Sr_{0.2}MnO_3$: *a* 0.1, *b* 0.2, and *c* 0.5 mA cm^{-2}

Table 1 Specific capacity of carbon in two kinds of catalyst

Catalyst	Specific capacity(mAh g^{-1}) at different rate (mA cm^{-2})		
	0.1	0.2	0.5
g-$La_{0.8}Sr_{0.2}MnO_3$	1,922	853	755
s-$La_{0.8}Sr_{0.2}MnO_3$	1,438	665	361

impurities existing in the s-$La_{0.8}Sr_{0.2}MnO_3$, even though there are no peaks of impurities can be found in the XRD pattern. For oxygen reduction reaction, the reduction peak potentials are −0.30 and −0.40 V for g-$La_{0.8}Sr_{0.2}MnO_3$ and s-$La_{0.8}Sr_{0.2}MnO_3$, respectively. It can be seen that the peak potential shifts positively by 0.10 V for g-$La_{0.8}Sr_{0.2}MnO_3$. Furthermore, peak current density for oxygen reduction on g-$La_{0.8}Sr_{0.2}MnO_3$ increase by 80% than that on s-$La_{0.8}Sr_{0.2}MnO_3$. The electrochemical results demonstrate that g-$La_{0.8}Sr_{0.2}MnO_3$ possesses higher electrocatalytic activity for oxygen reduction than s-$La_{0.8}Sr_{0.2}MnO_3$, which might be due to its larger specific surface area and smaller particle size.

Figure 4 presents the discharge behavior of Li-O_2 cells using the two kinds of $La_{0.8}Sr_{0.2}MnO_3$ materials as the air cathode catalysts. Curve (a) is the g-$La_{0.8}Sr_{0.2}MnO_3$ catalytic air cathode discharge at 0.1 mA cm^{-2}, curve (b) is the air cathode with s-$La_{0.8}Sr_{0.2}MnO_3$ at the same discharge rate. It can be seen from the discharge curves that the cells deliver a specific capacity at 1,900 mAh g^{-1} refer to carbon mass in curve (a) and about 1,200 mAh g^{-1} in curve (b), corresponding to 150% of that s-$La_{0.8}Sr_{0.2}MnO_3$ catalytic air cathode. What's more, the discharge plateau is about 2.6 V in curve (a) but in curve (b) is only 2.4 V, significantly showing that the voltage in curve (a) is more positive than (b) due to the higher catalytic activity catalyst decrease the polarization of oxygen reduction reaction. The standard potential for the discharge reaction U is 2.96 V which form the thermodynamics of the reaction. The over-potential η is given; all these demonstrate that the nano-catalyst of g-$La_{0.8}Sr_{0.2}MnO_3$ is prone to increase the capacity and has the ability to decrease the over potential and make the cell performance more superior. The reason is that the nano-sized $La_{0.8}Sr_{0.2}MnO_3$ has a larger surface area to provide more active sites, and catalytic sites determine the ORR polarization, resulting in higher voltage and less polarization. At the end of the discharge process, both the air cathode and the catalytic sites are clogged by lithium oxides, leading to polarization increase and voltage plateau decrease. At last, all the pore in the air cathode and catalytic sites are deactivated, leading to termination of discharge process.

Figures 5 and 6 show the discharge curves of Li–air battery catalyzed by two kinds of catalyst at different rates, increasing from 0.1 to 0.5 mA cm^{-2}. Figure 5 displays the discharge curves of air cathode catalyzed by g-$La_{0.8}Sr_{0.2}MnO_3$, average voltage decrease from 2.6 to 2.4 V as the discharge rate increase from 0.1 to 0.5 mA cm^{-2}, it delivered a specific capacity of 1,922 mAh g^{-1}, corresponding to 300% of that at 0.1 mA cm^{-2}. Figure 6 shows the discharge capacity of Li–air cell catalyzed by the s-$La_{0.8}Sr_{0.2}MnO_3$; there is an obviously decreasing trend of capacity for discharge rate from 0.1 to 0.5 mA cm^{-2}, the discharge capacity decreasing from 1,438 to 361 mAh g^{-1} at 0.1 mA cm^{-2} compared with that at 0.5 mA cm^{-2}. Table 1 summarizes the specific capacity of Li-air battery of two kinds of catalyst catalyzed air cathode at different current rates. It demonstrates that, at the same current rate, the g-$La_{0.8}Sr_{0.2}MnO_3$-catalyzed air cathode has a larger capacity, and with the increased in the current rate, the capacity decreases.

Conclusions

In summary, nano-sized $La_{0.8}Sr_{0.2}MnO_3$ was successfully synthesized with PEG-assisted sol–gel method. Comparing to the $La_{0.8}Sr_{0.2}MnO_3$ material prepared by the solid-state reaction method, it has a smaller uniform particle size, higher surface area (32 m^2 g^{-1}, respectively), and more purity. This suggests that the synthesis strategy used was effective. The g-$La_{0.8}Sr_{0.2}MnO_3$ catalyst has better catalytic activity than the s-$La_{0.8}Sr_{0.2}MnO_3$, which shows higher current peak of oxygen reduction reaction, and displays a higher specific capacity. It is obvious that high specific surface area catalyst will enhance the behavior, so changing the surface morphology into nanostructures to increase the electrochemical property is a promising way.

Acknowledgments This work was financially supported by the Natural Science Foundation of China (20873032) and Science and Technology Commission of Shanghai Municipality (08DZ2270500).

References

1. Ogasawara T, Debart A, Holzapfel M, Novak P, Bruce PG (2006) J Am Chem Soc 128:1390–1393
2. Gachot G, Grugeon S, Armand M, Pilard S, Guenot P, Tarascon JM, Laruelle S (2008) J Power Sources 178:409–421
3. Amalraj SF, Aurbach D (2011) J Solid State Electrochem 15:877–890
4. Leriche JB, Hamelet S, Shu J, Morcrette M, Masquelier C, Ouvrard G, Zerrouki M, Soudan P, Belin S, Elkaïm E, Baudelet F (2010) J Electrochem Soc 157:A606–A610
5. Jian Z, Wu X, Xiao H (2010) J Electrochem Soc 157:A940–A946
6. Abraham KM, Jiang Z (1996) J Electrochem Soc 143:1–5
7. Girishkumar, McCloskey B, Luntz AC, Swanson S, Wilcke W (2010) J Phys Chem Lett 1:2193–2203
8. Kraytsberg A, Eli YE (2011) J Power Sources 196:886–893
9. Laoire CO, Mukerjee S, Abraham KM (2010) J Phys Chem C 114:9178–9186
10. Debart A, Bao JL, Armstrong G, Bruce PG (2007) J Power Sources 174:1177–1182
11. Debart A, Bao JL, Armstrong G, Bruce PG (2008) Angew Chem Int Ed 47:4521–4524
12. Lu YC, Xu Z, Gasteiger HA, Chen S, Schifferli KH, Yang SH (2010) J Am Chem Soc 132:12170–12171
13. Ren X, Zhang SS, Tran DT, Read J (2011) J Mater Chem (in press)

14. Ohsaka T, Lanqun M, Arihara K, Sotomura T (2004) Electro Chem 6:273–277
15. Singh RN, Malviya M, Anindita, Sinba ASK, Chartier P (2007) Electrochim Acta 52:4264–4271
16. Sequeira CAC, Santos DMF, Brito PSD (2008) Russion J Electrochem 44:919–923
17. Hu ZG, Yang YY, Shang XL, Pang HL (2005) Mater Lett 59:1373–1377
18. Lu YC, Gasteiger HA, Crumlin E, McGuire R Jr, Yang SH (2010) J Electrochem Soc 157:A1016–A1025
19. Kang JW, Kim DH, Mathew V, Lim JS, Gim JH, Kim J (2011) J Electrochem Soc 158:A59–A62
20. Lee GH, Hoh SH, Jeong JW, Choi BJ, Kim SH, Ri HC (2002) J Am Chem Soc 124:12094–12095
21. Herbert G (1994) J Eur Ceram Soc 14:205–214
22. Kameli P, Salamati H, Aezami A (2008) J Alloys Compd 450:7–11
23. Grossin D, Noudem JG (2004) Solid State Sci 6:939–944
24. Miyazaki K, Sugimura N, Matsuoka K, Iriyama Y, Abe T, Matsuoka M, Ogumi Z (2008) J Power Sources 178:683–686